Chemical Geology 643 (2024) 121821

Contents lists available at ScienceDirect

Chemical Geology

journal homepage: www.elsevier.com/locate/chemgeo

Effect of mineral growth rate on Zinc incorporation into calcite and aragonite

Jean-Michel Brazier [a,*,1], Katja E. Goetschl [a], Martin Dietzel [a], Vasileios Mavromatis [b]

[a] Institute of Applied Geosciences, Graz University of Technology, Rechbauerstrasse 12, 8010 Graz, Austria
[b] Institute of Geological Sciences, University of Bern, Baltzerstrasse 1+3, 3012 Bern, Switzerland

ARTICLE INFO

Editor: Michael E. Boettcher

Keywords:
Zinc distribution coefficient
Calcite
Aragonite
Mineral growth rate

ABSTRACT

The distribution coefficient of Zn^{2+} (i.e., D_{Zn}^{2+}) between calcite/aragonite and reactive fluids were estimated as a function of mineral growth rate ($10^{-8.6} < r_p < 10^{-7.3}$ mol/m^2/s) at 25 °C and 1 bar pCO_2. The obtained results suggest that rate strongly influences D_{Zn}^{2+} in both minerals and the dependence of D_{Zn}^{2+} on growth rate can be described as:

Log $D_{Zn\,calcite}^{2+}$ = −0.331 (±0.048) Log r_p – 0.991 (±0.375); R^2 = 0.82

Log $D_{Zn\,aragonite}^{2+}$ = 0.751 (±0.089) Log r_p + 5.160 (±0.702); R^2 = 0.88

These correlations for calcite and aragonite are in agreement with the incorporation of foreign ions in compatible and incompatible host mineral structures, respectively. The use of the surface reaction kinetic model (SRKM) to fit the experimental data provided good results for calcite. In contrast, SRKM was not able to provide a good fit for Zn incorporation in aragonite, underlying the difficulties to model incorporation of foreign elements incompatible with the host mineral structure.

Moreover, a linear correlation was found between D_{Zn}^{2+} and the saturation degree of the reactive fluid with respect to the growing mineral phase that can be described as:

Log $D_{Zn\,calcite}^{2+}$ = −1.280 (±0.221) $SI_{calcite}$ + 1.864 (±0.053); R^2 = 0.77

Log $D_{Zn\,aragonite}^{2+}$ = 2.852 (±0.418) $SI_{aragonite}$ - 1.640 (±0.138); R^2 = 0.82

Considering that $SI_{mineral}$ = 0 reflects chemical equilibrium in the above equations, a Log D_{Zn}^{2+} at equilibrium was calculated for both calcite (1.9) and aragonite (−1.6). This value is in good agreement with the theoretical models for calcite, whereas in the case of aragonite it is 1.5 to 2.1 orders of magnitude lower than the previously published values. While the incorporation of Zn ions into calcite implies the formation of a dilute solid-solution between calcite and smithsonite (i.e. $ZnCO_3$), the incorporation of Zn ions into aragonite is likely associated to the density of defect sites at the growing mineral surface.

1. Introduction

The presence of foreign ions in carbonate minerals offers an excellent opportunity to reconstruct the (paleo)physicochemical conditions of their formation medium by elucidating the reactions and mechanisms controlling their incorporation into the solid phase (e.g., Kitano et al., 1975; Lorens, 1981; Mucci and Morse, 1983; Dromgoole and Walter, 1990; Paquette and Reeder, 1995; Reeder, 1996; Dietzel et al., 2004; Gaetani and Cohen, 2006; Lee and Reeder, 2006; Lakshtanov and Stipp, 2007; Gabitov et al., 2008, 2011, 2021; Mavromatis et al., 2013, 2018, 2022; Alvarez et al., 2021; Brazier and Mavromatis, 2022). The abundance and ubiquity of the thermodynamically stable $CaCO_3$ polymorph calcite under ambient conditions explains the particular attention it has received and the motivation in using it as (paleo) environmental proxy. It has been demonstrated experimentally that temperature, pH, saturation state of the reactive fluid with respect to the forming mineral, or mineral growth rate exert control on the foreign ion incorporation into carbonate minerals (e.g., Morse and Bender, 1990; Temmam et al., 2000; Tang et al., 2008; Mavromatis et al., 2015; Voigt et al., 2017; Füger et al., 2019; Goetschl et al., 2019). In contrast, the parameters controlling foreign ions incorporation in aragonite have not been adequately explored and only few studies have shown that the

* Corresponding author.
E-mail address: jean-michel.brazier@unibe.ch (J.-M. Brazier).
[1] Current address: Institute of Geological Sciences, University of Bern, Baltzerstrasse 1+3, 3012 Bern, Switzerland.

https://doi.org/10.1016/j.chemgeo.2023.121821
Received 15 March 2023; Received in revised form 31 October 2023; Accepted 7 November 2023
Available online 9 November 2023

foreign to Ca ions molar ratio in aragonite are highly valuable for environmental reconstruction purposes (Raiswell and Brimblecombe, 1977; White, 1977; Terakado and Masuda, 1988; Dietzel et al., 2004; Gaetani and Cohen, 2006; Gabitov et al., 2008; Mavromatis et al., 2018, 2022; Brazier and Mavromatis, 2022; Brazier et al., 2023).

In contrast to calcite, which crystallizes in the trigonal system, aragonite crystallizes in the orthorhombic system and in this phase Ca^{2+} is coordinated to 9 oxygen ions. In this coordination system an ion-by-ion substitution with foreign cations with smaller radii than Ca^{2+} is not favourable. This incompatibility of smaller cations substituting $Ca^{[9]}$ in the aragonite structure was reflected by the <1 distribution coefficient between the solid and the reactive fluid defined as:

$$D^{*}_{Me^{2+}} = \frac{(C_{Me}/C_{Ca})_{solid}}{(a_{Me^{2+}}/a_{Ca^{2+}})_{fluid}} \quad (1)$$

where C and a stand for molar concentration and activity of free ions, respectively. Notably, the incorporation of foreign elements into an incompatible crystal structure (i.e., lack of dilute solid-solution formation) has not been thoroughly studied and gaps of fundamental understanding related to reaction kinetics and mechanisms controlling ion incorporation still remain.

Zinc is an element of interest due to its main role in oceanic biological cycles where it is an essential micronutrient for biotas (e.g., DNA replication and transcription, cofactor in carbonic anhydrase and alkaline phosphatase enzymes). Although Zn plays an essential role in many biochemical systems when present at low concentrations, it can become toxic at very high concentrations (e.g., Fisher et al., 1981; Morel and Price, 2003; Bruland and Lohan, 2006; Rout and Das, 2009; Bong et al., 2010; Conway and John, 2014; Weber et al., 2018; Kaur and Garg, 2021). Similar to other divalent transition metals, Zn ions show a high affinity for adsorption on solid surfaces and for incorporation into calcite (Crocket and Winchester, 1966; Kitano et al., 1976; Zachara et al., 1989; Reeder, 1996; Cheng et al., 1998; Dong and Wasylenki, 2016; van Dijk et al., 2017; Mavromatis et al., 2019). Interestingly, Zn ions have a strong ability to change their coordination with respect to oxygen ions both in aqueous fluid and when adsorbed at or incorporated into a solid. Previous studies have shown, that although zinc adsorbs onto the surface of calcite as a tetrahedrally coordinated complex, its coordination number is smaller (between 2 and 4-fold coordination) compared to the crystal lattice (6-fold coordination) (e.g., Elzinga and Reeder, 2002; Burgess and Prince, 2006; Elzinga et al., 2006; Fujii et al., 2014). This ability to reach a 6-fold coordination in the calcite crystal lattice as well as the very high distribution coefficient ($D^{2+}_{Zn|cite}$) are consistent with an ion-by-ion substitution of Zn^{2+} with Ca^{2+} ions, indicating the formation of a dilute solid-solution between calcite and smithsonite ($ZnCO_3$) (Reeder et al., 1999). However, in order Zn^{2+} to substitute $Ca^{[9]}$ in aragonite lattice requires a coordination change from 6 in the fluid to 9 in the solid. This coordination change together with the significant small ionic radius of Zn^{2+} compared to $Ca^{[9]}$ makes this substitution unfavourable. While some studies focused on the Zn adsorption/incorporation in calcite from an isotopic point of view (e.g., Dong and Wasylenki, 2016; Mavromatis et al., 2019), to our knowledge only few studies have focused on the parameters controlling the elemental incorporation of zinc into calcite or aragonite.

In this study, we explore the effect of mineral growth rate on Zn incorporation into calcite and aragonite through co-precipitation experiments (25 °C and 1 bar pCO_2) using the constant addition technique. The obtained results bring insights into the effect of mineral growth rate on Zn distribution between both calcite and aragonite and forming fluid and represent a case scenario for an element incorporation into a compatible and incompatible crystal structure.

2. Materials and methods

2.1. Incorporation experiments

The incorporation of Zn into calcite and aragonite was studied during mineral overgrowth on synthetic seeds of calcite (from Sigma-Aldrich) and aragonite (precipitated following the procedure of Mavromatis et al. (2022)) using a mixed flow reactor (see Fig. 1; previously described by Mavromatis et al., 2019). The experiments were performed at 25 °C and 1 bar pCO_2 to ensure that the majority of aqueous Zn is present as free ions (i.e. Zn^{2+}) in the reactive fluids and to avoid the formation of hydrozincite (i.e., $Zn_5(CO_3)_2(OH)_6$). The use of a NO_3^- matrix instead of Cl^- has been chosen due to the smaller affinity for aquo-complex formation of Zn^{2+} with NO_3^- compared to Cl^- (i.e., Mavromatis et al., 2019). Shortly before the onset of the experiments, 0.5 L of fluid containing $Zn(NO_3)_2$ (~0.5 mM and ~0.25 mM for calcite and aragonite experiments, respectively), ~300 mM of $NaNO_3$ and ~10 mM of $Ca(NO_3)_2$ were prepared for each reactor. Note that ~25 mM of $Mg(NO_3)_2$ was added during the experiments with aragonite seeds to inhibit formation and growth of calcite (e.g., Bischoff, 1968; Berner, 1975). Between 1 and 5 g of seeds were added to each reactor at the beginning of the experiments and the homogeneity of the mixture was ensured by continuous stirring at 240 rpm with Teflon coated floating stirring bars. Calcite and aragonite overgrowth in the reactors was induced by the introduction via a peristaltic pump at similar flowrates (i.e., between 10.4 and 22.7 mL/day) of two distinct inlet fluids (fluid 1: $Ca(NO_3)_2$, $Zn(NO_3)_2$ (and $Mg(NO_3)_2$ for experiments with aragonite); fluid 2: Na_2CO_3 and $NaNO_3$). To avoid concentrations modification in the reactive fluid due to dilution effect, the concentrations of $Zn(NO_3)_2$, $NaNO_3$ and $Mg(NO_3)_2$ in the inlet fluid were double to the initial reactive fluid. The concentrations of $Ca(NO_3)_2$ and Na_2CO_3 of the inlet fluids varied between 60 and 150 mM among separate experiments to investigate a broad range of mineral growth rate. All reactive fluids were prepared from analytical grade chemicals and deionized water (Millipore Integral 3; 18.2 mΩ/cm). The pH of the reactive fluid (i.e., $6.2 \leq pH \leq 6.5$) was controlled by continuous bubbling of pure wet CO_2 (prior bubble through deionized water to reduce evaporation) into the reactive fluids. Due to the pumping of inlet fluids in the reactors, the volume of the reactive fluid increased by ~20 mL per time unit (i.e., 12 or 24 h) and a similar volume was then sampled in order to keep the volume constant within a ± 4% range. Prior to supernatant sampling, the stirring was paused to let the solid settle down to minimize solid removal and to keep the solid/fluid ratio within the same ± 4% variation range. The samples were then filtered through 0.2 μm cellulose acetate syringe filters (VWR) and the pH was measured therein. One sub-sample was used to determine the total alkalinity and the rest was acidified with bi-distilled 14 N HNO_3 and stored at 4 °C for wet chemical analyses. Experiments were concluded by the complete vacuum filtration of the reactive fluids through 0.2 μm cellulose acetate filters (Sartorius). The recovered solids were rinsed with deionized water and dried at 40 °C.

2.2. Mineralogic and wet chemical analyses

The seed material and solids recovered at the end of each experiment were characterized by X-ray diffraction (XRD) using a PANalytical X'Pert PRO diffractometer and a Co-Kα radiation (40 mA, 40 kV) scanning a 2θ range of 4–85° at 0.03° s^{-1}. Rietveld refinement was performed on the PANalytical Highscore Plus software together with the ISCD database to quantify the mineral phases in presence within 1 wt% error. Solid samples were gold-coated before acquisition of scanning electron microscope (SEM) images on a Zeiss DSM 92 Gemini SEM operating at 5 kV acceleration voltage. The specific surface areas of the seeds and solids recovered at the end of each experiment were determined by BET method (Brunauer et al., 1938) on a Micromeritics Tristar II plus analyser and on a Quantachrome Gas Sorption system both using 11-points krypton adsorption. The chemical composition of the solids (i.

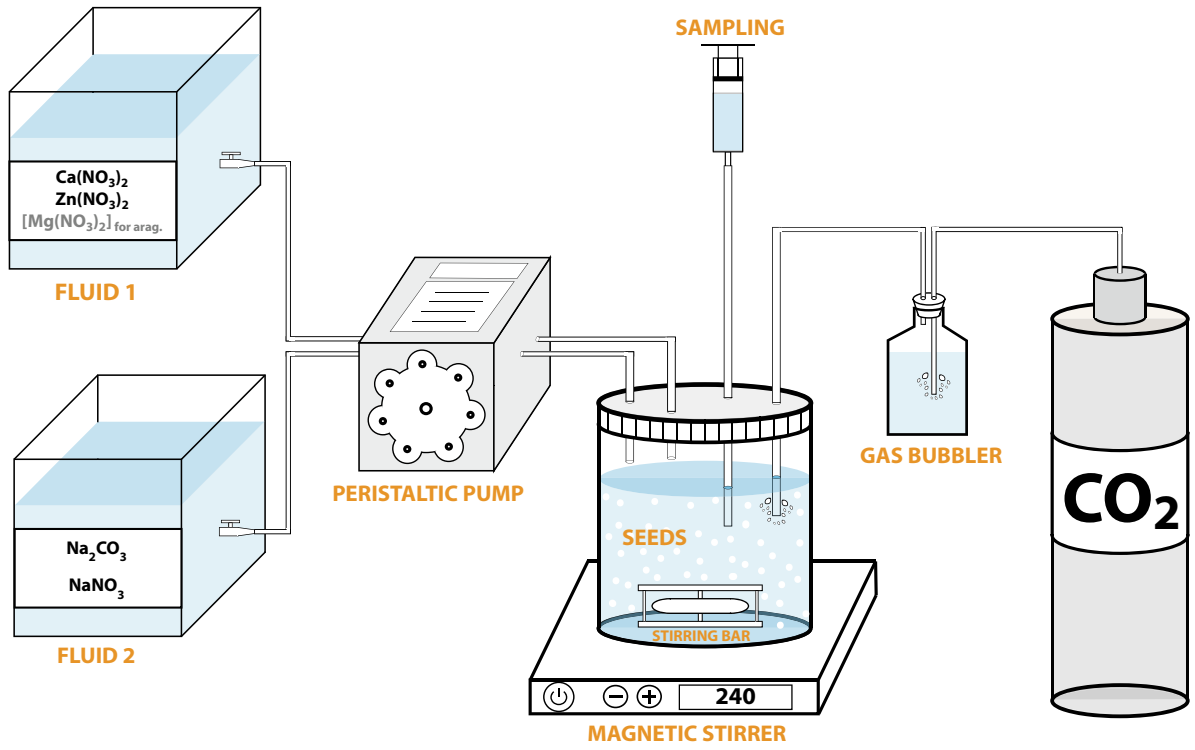

Fig. 1. Experimental setup for the calcite and aragonite mineral growth experiments with zinc ion incorporation.

e., Ca and Zn concentrations) was measured on an Agilent 7500CX inductively coupled plasma mass spectrometer (ICP-MS), with a matrix-matched calibration and a precision better than 3% (RSD), after digestion of ~80 mg of each sample in 2% HNO_3 (prepared from bi-distilled acid). The instrumental drift was corrected by internal standard normalization using a mixture of Sc, Se and Ge, while the accuracy was ensured by repeated measurements of SPS-SW1 and XXI solution standards.

The pH of the filtered fluids was measured with a SenTix 945 Gel pH electrode (WTW) calibrated with three NIST buffers (pH 4.01, 7.00 and 10.01), and the total alkalinity was measured on a TitroLine alpha plus (Schott) by titration of 10 mM HCl with an analytical precision of ±2%. The concentrations of Na were measured on a Perkim Elmer Optima 8300 DV inductively coupled plasma optical emission spectrometer (ICP-OES) with a precision better than 3% (RSD), while Zn, Ca and Mg concentrations were measured on an Agilent 7500CX ICP-MS following the same procedure described above. The aqueous speciation, ions activities and saturation indices (SI = Log (IAP/K_{sp})) of the reactive fluids with respect to calcite and aragonite were calculated using the PHREEQC v.3 software together with the MINTEQ.V4 database (Parkhurst and Appelo, 2013), after the addition of the solubility products of nesquehonite [$MgCO_3.3H_2O$] and dypingite [$Mg_5(CO_3)_4(OH)_2.5H_2O$] from Harrison et al. (2019), hydromagnesite [$Mg_5(CO_3)_4(OH)_2.4H_2O$] from Gautier et al. (2014), magnesite [$MgCO_3$] from Bénézeth et al. (2011), and hydrozincite [$Zn_5(CO_3)_2(OH)_6$] that was adapted from the llnl database. Speciation of Ca and Zn during the experiments are given in Table A.1.

3. Results

3.1. Mineralogy and chemical composition of the solids

X-ray diffraction patterns indicate that calcite seeds consist of 100 wt % of calcite, while aragonite seeds contain 98.5 wt% of aragonite and 1.5 wt% of calcite. In the case of the calcite experiments, the overgrowths are composed exclusively of calcite, while for the aragonite experiments, the post-experiment solids are composed mainly of aragonite with traces of calcite (< 1.5 wt%), which systematically occurs in lower proportion than in the seeds indicating an exclusive aragonite growth. SEM observations show rhombohedral calcite seeds consisting of 5 to 15 μm grains and aragonite seeds consisting of needle-shape grains of 20–80 μm length and 2–10 μm diameter (Fig. 2A–B). In both cases, the SEM analyses of the solids after the experiments show step and islands surface structures consistent with mineral overgrowth

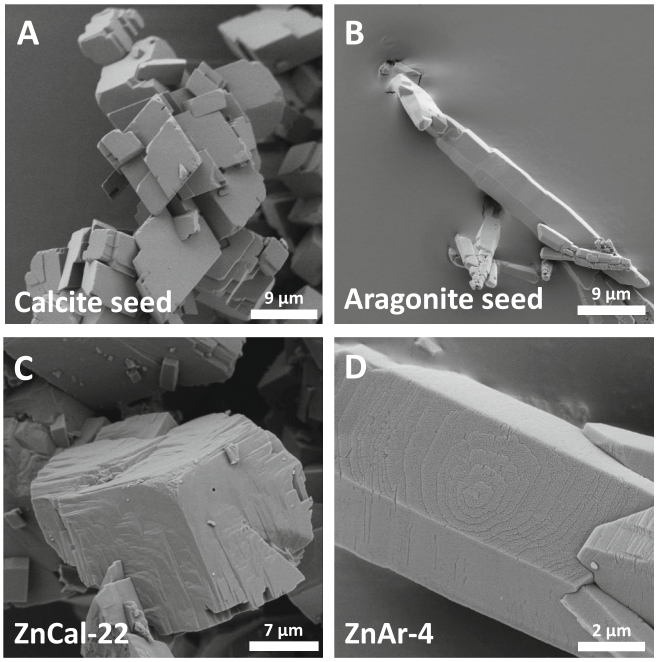

Fig. 2. Scanning electron microscope (SEM) images of (A) the calcite and (B) the aragonite seeds used in this study, (C) overgrown calcite from experiment ZnCal-22, and (D) overgrown aragonite from experiment ZnAr-4.

(Fig. 2C–D). The amount of overgrowth in each experimental run under steady state conditions can be estimated through the equation:

$$Overgrowth = [[(nCa_{add}) - (nCa_{rem})] - M_{carbonate}] \times N_{days} \quad (2)$$

where nCa_{add} and nCa_{rem} are the number of moles of Ca added into and removed from the reactor over 24 h, respectively, $M_{carbonate}$ is the molar mass of calcium carbonate in g/mol (i.e., 100.0869 g/mol), and N_{days} is the duration of the experiments in days. The BET specific surface areas were measured at 0.17 and 0.50 g/m^2 for the calcite and the aragonite seeds, respectively, while slightly different values were measured in the solid after experiments and taking into consideration in calculations. Concentration measurements performed on five separate digestions of each seed revealed that neither the calcite nor the aragonite seeds contained zinc. The Zn/Ca ratios in calcite and aragonite overgrowths were calculated following mass balance considerations and are expressed in mmol/mol in the Table 1. For the calcite overgrowth, the Zn/Ca varied between 9.6 and 25.6 mmol/mol, while the values for the aragonite overgrowth exhibited far lower values between 0.7 and 3.5 mmol/mol.

3.2. Composition of the reactive fluid

An example of the temporal evolution of pH, Ca and Zn (and Mg in the case of aragonite) concentrations in the reactive fluids can be seen in Fig. 3A–B for the experiments ZnCal-32 and ZnAr-7, respectively. Chemical steady-state conditions are attained after one day for pH and Ca concentration in the fluid reacting with calcite, while the concentration of Zn needs in average 8 days to reach steady-state (10 days in the ZnCal-32 example). On the other hand, the pH, Ca, Mg and Zn concentration of the fluids reacting with aragonite reach steady-state conditions after one day.

Table 1
pH of the reactive fluids, Zn/Ca ratio in the precipitated solids, saturation indices of the reactive fluids with respect to calcite and aragonite at steady state (i.e., $SI_{calcite}$ and $SI_{aragonite}$), growth rate (Log r_p), distribution coefficient of Zn (Log D^{2+}_{Zn}) between the calcite/aragonite and the reactive fluid at steady state.

Experiments	Mineral phase	pH	Zn/Ca (mmol/mol)	$SI_{calcite}$	Log r_p (mol/m^2/s)	Log $D^{2+}_{Zncalcite}$
ZnCal-20	Calcite	6.23	17.8	0.21	−7.9	1.6
ZnCal-22	Calcite	6.26	14.0	0.27	−7.7	1.6
ZnCal-23	Calcite	6.24	13.5	0.24	−7.8	1.6
ZnCal-24	Calcite	6.30	9.9	0.31	−7.5	1.5
ZnCal-32	Calcite	6.26	18.0	0.19	−8.0	1.6
ZnCal-34	Calcite	6.23	13.4	0.16	−7.9	1.6
ZnCal-35	Calcite	6.24	13.1	0.15	−8.0	1.7
ZnCal-36	Calcite	6.26	9.6	0.21	−7.8	1.6
ZnCal-44	Calcite	6.29	18.1	0.25	−7.6	1.6
ZnCal-45	Calcite	6.29	25.6	0.22	−7.7	1.6
ZnCal-46	Calcite	6.32	13.2	0.26	−7.4	1.5
ZnCal-47	Calcite	6.33	13.5	0.31	−7.5	1.4

Experiments	Mineral phase	pH	Zn/Ca (mmol/mol)	$SI_{aragonite}$	Log r_p (mol/m^2/s)	Log $D^{2+}_{Znaragonite}$
ZnAr-1	Aragonite	6.34	1.1	0.19	−8.1	−0.9
ZnAr-2	Aragonite	6.39	2.5	0.42	−7.5	−0.5
ZnAr-3	Aragonite	6.37	2.0	0.34	−7.5	−0.6
ZnAr-4	Aragonite	6.38	1.8	0.34	−7.7	−0.6
ZnAr-5	Aragonite	6.37	1.2	0.27	−7.8	−0.8
ZnAr-6	Aragonite	6.43	3.5	0.44	−7.3	−0.2
ZnAr-7	Aragonite	6.35	0.7	0.18	−8.6	−1.2
ZnAr-8	Aragonite	6.45	1.1	0.35	−8.0	−0.9
ZnAr-9	Aragonite	6.39	0.9	0.22	−8.2	−1.0
ZnAr-10	Aragonite	6.45	2.5	0.43	−7.7	−0.4
ZnAr-11	Aragonite	6.45	1.4	0.34	−7.9	−0.8
ZnAr-12	Aragonite	6.44	1.6	0.32	−7.8	−0.7

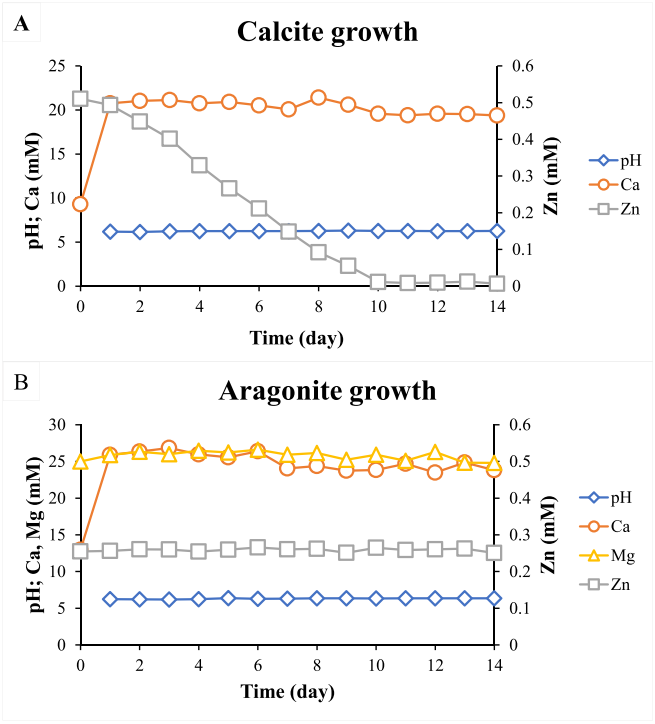

Fig. 3. Example of evolution of pH, Ca and Zn concentrations (and Mg for aragonite) of the reactive fluids as a function of reaction time for (A) calcite growth (exp. ZnCal-32) and (B) aragonite growth (exp. ZnAr-7) experiments.

Under steady-state conditions, the growth rate (in mol/m^2/s) can be estimated by mass balance considerations as:

$$r_p = \frac{\frac{((nCa_{add}+nZn_{add})-(nCa_{rem}+nZn_{rem}))}{86400}}{S} \quad (3)$$

where nCa$_{add}$, nZn$_{add}$, nCa$_{rem}$ and nZn$_{rem}$ are the number of moles of Ca and Zn added and removed by time unit (i.e., 24 h), respectively, 86,400 is the number of second in 24 h and S is the specific surface area of the recovered solid in m^2 (see Table A.2). It has to be noted that (i) the specific surface area of the minerals recovered after overgrowth experiments were slightly different than the one of the seeds and that correction were thus accordingly applied in Eq. (3) and (ii) the Zn was integrated in this calculation but has a very limited influence of the r_p value due to the large difference in concentrations between Ca and Zn in both inlet and reactive fluids. The overall ranges of growth rate investigated in this study were $-8.0 \leq \text{Log } r_p \leq -7.4$ and $-8.6 \leq \text{Log } r_p \leq -7.3$ for calcite and aragonite, respectively.

3.3. Zinc distribution between mineral and the reactive fluid

The distribution coefficient of divalent cations (D^{2+}_{Me}, see Eq. (1)) in $CaCO_3$ minerals is usually based on the assumption that the presence of Me^{2+} in the minerals is the result of an incorporation of free ions in the growing mineral surface (Burton et al., 1951), leading to (i) an ion-by-ion substitution of Ca^{2+} by Me^{2+} and (ii) the formation of a diluted solid-solution between $CaCO_3$ and $MeCO_3$ endmembers (e.g., Dromgoole and Walter, 1990; Tesoriero and Pankow, 1996; Mavromatis et al., 2013, 2018; Brazier and Mavromatis, 2022). Although formation of such an ideal solid-solution is rather unlikely to occur between $ZnCO_3$ and aragonite, the use of Eq. (1) allows a direct comparison of the D^{2+}_{Zn} between calcite and aragonite. For the experiments performed in the presence of aragonite, the Eq. (1) was applied directly. Since the Zn concentration in the reactive fluid from which calcite forms requires several days to achieve steady-state conditions, the equation used to calculate the Zn distribution coefficient has been adapted from

Mavromatis et al. (2019) and is based on mass balance consideration of Zn concentration in the reactive fluids and is defined as:

$$D^{*}_{Zn^{2+}} = \frac{\left(\frac{n_{Zn\ added} - \left(F_r \times [Zn]_{steady-state}\right)}{n_{Ca\ added} - \left(F_r \times [Ca]_{steady-state}\right)}\right)_{solid}}{\left(a_{Zn^{2+}}/a_{Ca^{2+}}\right)_{fluid}} \quad (4)$$

where $n_{Zn\ added}$ and $n_{Ca\ added}$ are the mole of Zn and Ca added to the reactive fluid per unit of time, F_r is the flowrate in mL per unit of time, and $[Zn]_{steady\text{-}state}$ and $[Ca]_{steady\text{-}state}$ are the Zn and Ca concentrations of the reactive fluid at steady-state, respectively. Since a large proportion of Zn in the reactive fluid is complexed with NO_3^- and HCO_3^- (see Table A.1), the activities of Zn^{2+}were used in Eqs. (1) and (4) to ensure that the calculated distribution coefficients are not affected by chemical speciation.

The Log D^{2+}_{Zn} values can be found in Table 1 and range from 1.4 to 1.7 for calcite, and from −1.2 to −0.2 for aragonite. Interestingly, a linear dependency between Log D^{2+}_{Zn} and mineral growth rate exist (see Fig. 4A–B) for both calcite and aragonite, and can described by the equations:

$$\text{Log } D^{*}_{Zn^{2+},calcite} = -0.331\ (\pm 0.048)\ \text{Log } r_p - 0.991\ (\pm 0.375);\ R^2 = 0.82 \quad (5)$$

$$\text{Log } D^{*}_{Zn^{2+},aragonite} = 0.751\ (\pm 0.089)\ \text{Log } r_p + 5.160\ (\pm 0.702);\ R^2 = 0.88 \quad (6)$$

and are valid for the experimental conditions explored in this study (i.e., temperature, ionic strength, pCO_2, growth rate). Detailed results about the experiments can be found in Table A.2.

4. Discussion

4.1. Zinc incorporation in calcite

A limited negative correlation exists between D^{2+}_{Zn} and calcite growth rate (see Fig. 4A) with a decrease of Log $D^{2+}_{Zn\ calcite}$ of ~0.3 orders of magnitude (from 1.7 to 1.4) for a Log r_p increase of ~0.6 orders of magnitude (from −8.0 to −7.4 mol/m^2/s). This behaviour is consistent with the incorporation of elements into a compatible mineral structure. Similar behaviour has been demonstrated experimentally for several

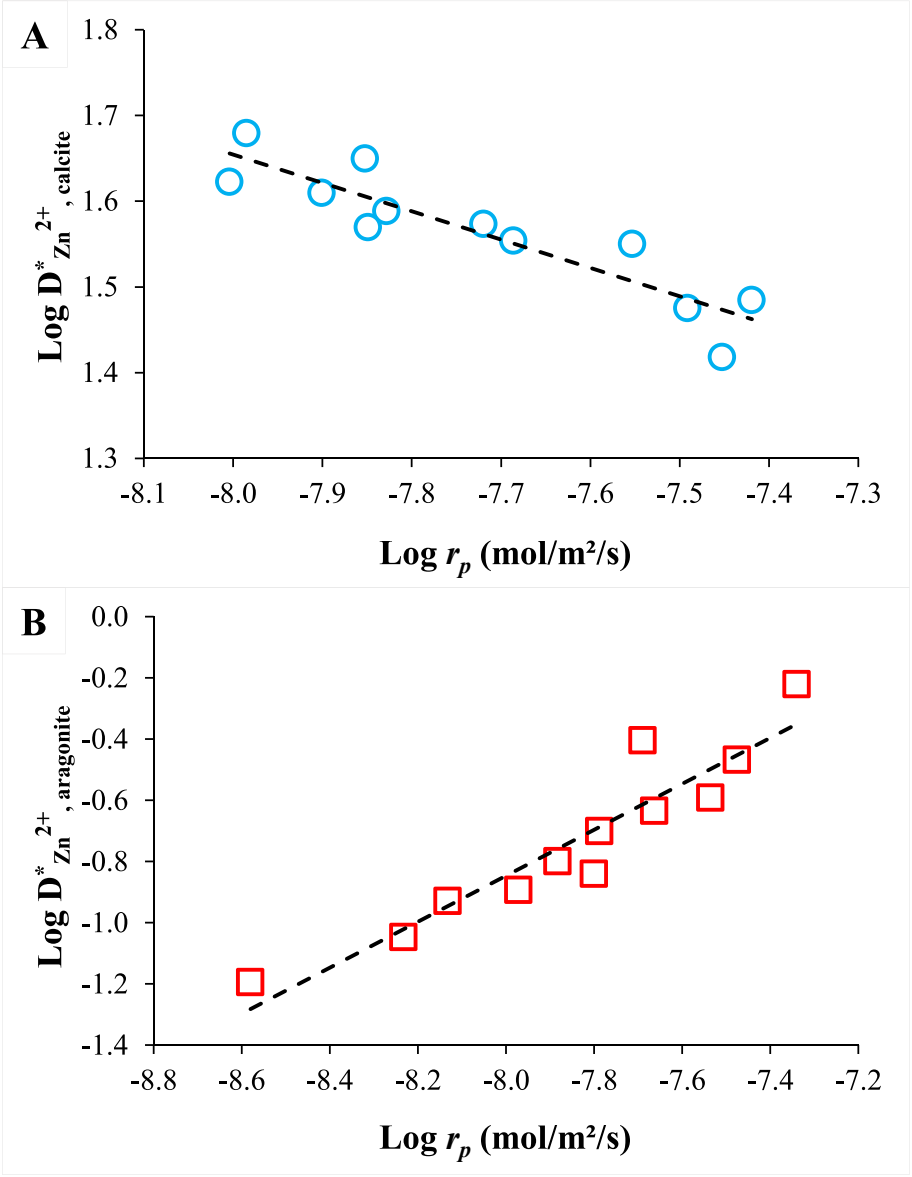

Fig. 4. Dependence of the distribution coefficient (A) Log $D^{2+}_{Zncalcite}$ and (B) Log D^{2+}_{Zn}aragonite on growth rate (Log r_p) (see Eqs. 5 and 6, respectively).

elements during their incorporation into calcite (e.g., Fe, Mn, Ni, Co, Cd, REE) or aragonite (e.g., Sr) (Kitano et al., 1980; Lorens, 1981; Dromgoole and Walter,1990; Tesoriero and Pankow, 1996; Lee and Reeder, 2006; Lakshtanov and Stipp, 2007; Voigt et al., 2017). Only few experimental data exist regarding the distribution coefficient of Zn in calcite but it is worth mentioning here Kitano et al. (1973, 1980) who determined values of Log $D^{2+}_{Zn\ calcite}$ between 1.2 and 1.7 or Mavromatis et al. (2019) with values between 1.0 and 1.5. Interestingly, the latter distribution coefficients are rather similar than those obtained in the present study for the same pH and growth rate ranges. Paquette and Reeder (1995) and Reeder (1996) have shown that the incorporation of trace elements depends on the ionic radius of each element but also on the size and geometry of the incorporation sites in the growth steps and kinks, which themselves are associated with the morphology of the crystal faces on which they grow. Reeder (1996) showed that Zn has a different behaviour than other transition metals (e.g., Co) and that mechanisms such as site-specific adsorption, dehydration, desorption effects after partial incorporation or ionic complexes interacting with mineral surfaces have to be considered. These results were later completed by Elzinga and Reeder (2002) who showed by EXAFS analyses that the geometry of the adsorbed complexes is fundamental in the incorporation of foreign elements in calcite. For example, Zn ions are adsorbed as a tetrahedral complexes which appears to be favourable for adsorption and incorporation into the <−441>+ steps. In any case, it appears that the growth step velocity, and thus the growth rate, is a determining factor in the incorporation of Zn into calcite (Reeder, 1996).

Due to the correlation of growth rate on saturation index (see Fig. A.1), the obtained results also show a strong correlation between the Log $D^{2+}_{Zn\ calcite}$ and the SI of the reactive fluids with respect to calcite (See Fig. 5A) which can be numerically described as:

$$\text{Log } D^{*\ 2+}_{Zn\ calcite} = -1.280\ (\pm 0.225)\ SI_{calcite} + 1.864\ (\pm 0.053);\ R^2 = 0.77 \quad (7)$$

This linear trend allows to estimate a value of Log $D^{2+}_{Zn\ calcite}$ at equilibrium if it is assumed that at $SI_{calcite} = 0$ the D^{2+}_{Zn} value reflects equilibrium conditions. Accordingly, a value of Log $D^{2+}_{Zncite,\ eq} = 1.9$ was calculated. Using a different approach, several studies estimated the Log $D^{2+}_{Zncite,\ eq}$ values for calcite following different modelling approaches. Böttcher and Dietzel (2010), in an approach correlating the solubility products of the end-members, show an estimated value of Log $D^{2+}_{Zncite,\ eq}$ of 1.4, which is lower than the estimated value in this study. A part of this difference could result from uncertainty in the estimation of the solubility products of smithsonite and/or calcite. Using the K_{sp} values proposed in the PHREEQC MINTEQ.v4 database (i.e., Log $K_{sp} = -8.48$ and − 10.00 for calcite and smithsonite, respectively), it is possible to calculate a $D^{2+}_{Zncite,\ eq}$ following the equation:

$$D^{*}_{Zn^{2+}_{calcite,eq}} = \frac{K_{sp,calcite}}{K_{sp,smithsonite}} \quad (8)$$

where $K_{sp,\ calcite}$ and $K_{sp,\ smithsonite}$ are the solubility products of calcite and smithsonite, respectively. A Log $D^{2+}_{Zncite,\ eq}$ value of 1.5 can be calculated, which is a bit closer to the results of this study compared to those presented by Böttcher and Dietzel (2010). In their review article, Rimstidt et al. (1998) have shown that theoretical distribution coefficients differ from experimental distribution coefficients because experiments can only approximate equilibrium conditions and thus kinetic processes still produce non-uniform distributions of foreign elements in freshly precipitated minerals. To solve this discrepancy, they proposed an approach based on the McIntire equations (McIntire, 1963). Through a linear correlation including experimental results for different elements, they proposed a calculation of the $D^{2+}_{Zncite,\ eq}$ as:

$$D^{*}_{Zn^{2+}_{eq}} = 1.6\left(\frac{K_{sp,calcite}}{K_{sp,smithsonite}}\right)^{x} \quad (9)$$

where x is a kinetic factor that obtains a value of 1 under equilibrium conditions. Following this calculation, they proposed Log $D^{2+}_{Zncite,\ eq}$ value of 2.1, which is slightly higher than the value calculated in this work. Two sources of uncertainty contribute to the differences between the result obtained with Eq. (9) and those obtained herein. The first related to the K_{sp} values for calcite and smithsonite that were used by Rimstidt et al. (1998) which are different from the values proposed in the MINTEQ.v4 database. Actually, by using the latter in the Eq. (9), a value of Log $D^{2+}_{Zncite,\ eq}$ of 1.7 can be estimated, which is in good agreement to the results of this work. The second source of uncertainty is related to the experimental data that Rimstidt et al. (1998) used to establish the linearity between the distribution coefficient and the solubility product ratio. Indeed, the experimental conditions of the earlier studies are completely different from those applied herein (difference in pH, ionic strength, background electrolyte) which could possibly lead to a correlation factor of 1.6 that is not valid for our experiments.

Finally, Wang and Xu (2001) estimated a Log $D^{2+}_{Zncite,\ eq}$ value using an approach that correlates the difference in the standard Gibbs free energy of formation, the difference in the standard non-solvation energy and the difference in ionic radius between the foreign and the host element (Zn^{2+} and Ca^{2+}, respectively). The value estimated in their model (Log $D^{2+}_{Zncite,\ eq} = 0.6$) is significantly lower than every other work. The difficulties to predict the elemental distribution coefficient between minerals and reactive fluids, even in the case of foreign elements compatible with the structure of the considered mineral, underline our limited knowledge of the mechanisms controlling the incorporation and the difficulty to approach the activity of the Zn ions in the solid.

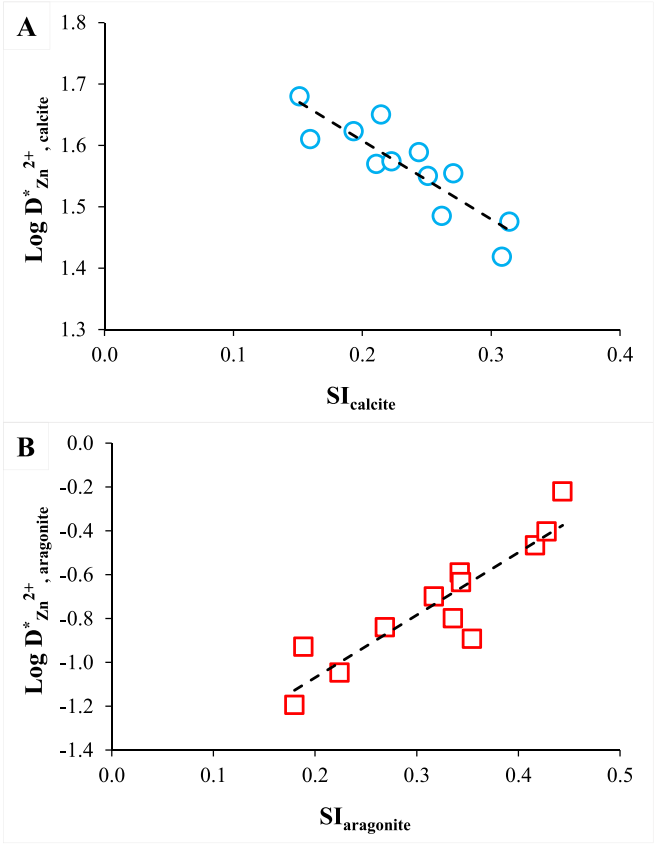

Fig. 5. Dependence of the distribution coefficient (A) $D^{2+}_{Zncalcite}$ and (B) Log $D^{2+}_{Zn\ aragonite}$ on the saturation index (SI) of the reactive fluid with respect to the calcite and aragonite, respectively (see Eqs. 7 and 10).

4.2. Zinc incorporation in aragonite

The incorporation of Zn in aragonite is characterized by a positive correlation between Log $D^{2+}_{Zn\ aragonite}$ and Log r_p. This positive correlation as well as the Log $D^{2+}_{Zn\ aragonite}$ values reported in this work suggest that during its incorporation in aragonite, Zn behaves as an incompatible element to this crystal structure. Similar trends have already been reported for several mono- and di-valent ions when incorporated into aragonite (e.g., Na^+, K^+, Ba^{2+}, Mg^{2+}, Ni^{2+}, Co^{2+}; White, 1977; Mavromatis et al., 2018, 2022; Brazier and Mavromatis, 2022). Several mechanisms have been proposed to explain the incompatibility of these ions into the aragonite structure including differences in ionic radii between the foreign and host elements (i.e., Ca^{2+}), the inability to fulfil the 9-fold coordination of the aragonite structure, the hydration energy and the rate of water molecule exchange in the hydration shell. Furthermore, similar to the incorporation of Zn into calcite, a strong linear correlation between the Log $D^{2+}_{Zn\ aragonite}$ and $SI_{aragonite}$ exists (Fig. 5B) and can be mathematically described as:

$$\text{Log } D^{*\ 2+}_{Zn\ aragonite} = 2.852\ (\pm 0.418)\ SI_{aragonite} - 1.640\ (\pm 0.138);\ R^2 = 0.82 \quad (10)$$

Following Eq. (10), it is thus possible to estimate a Log $D^{2+}_{aragonite,\ eq} = -1.6$ when $SI_{aragonite} = 0$, a value that reflects equilibrium conditions.

To our knowledge, 9-fold coordinated Zn^{2+} has never been documented, making it impossible to compare its ionic radius size with the one of the 9-fold coordinated Ca^{2+} in the aragonite crystal structure. Nevertheless, it appears that its ionic radius is ~26% smaller than the one of Ca^{2+} for similar coordination number (i.e., 0.74 vs 1.00 Å in 6-fold coordination, respectively; Shannon, 1976). This small ionic radius compared to that of Ca^{2+} does not allow Zn^{2+} to fulfil the 9-fold coordination of the aragonite crystal structure, which explains why smithsonite ($ZnCO_3$), which is the pure Zn-bearing carbonate phase, has a crystal structure similar to that of calcite (Frost et al., 2008). Comparing the obtained results with the distribution of two other transition metal ions (Ni^{2+} and Co^{2+}) in aragonite under similar conditions, it is interesting to note that the ionic radius of Zn^{2+} in 6-fold coordination (i.e., 0.74 Å) is intermediate to that of Ni^{2+} and Co^{2+} in the same coordination (i.e., 0.69 and 0.745 Å) and similarly shows a Log $D^{2+}_{aragonite,\ eq}$ value intermediate (−1.6) to that found for Ni^{2+} (−3.9) and Co^{2+} (−1.0) (Brazier and Mavromatis, 2022). This observation agrees with the observations of Okumura and Kitano (1986) who showed, in the case of monovalent ions, that incorporation increases in aragonite as the ionic radius of the foreign ion approaches that of Ca^{2+}.

Beyond the ionic radius and the ability to change coordination between the aqueous and solid phase, it appears that the hydration energy and the exchange rate of water molecules in the hydration shell of the considered cations are also parameters that influence the incorporation of foreign elements into minerals. Zinc is a highly hydrated ion (9.6 molecule of water in its shell) and has a strong affinity for the liquid phase which is underlined by its low Gibbs free energy of hydration (−1955 kJ/mol) (Marcus, 1991). Interestingly, these values are intermediate to those found for example for Ni^{2+} (10.4 molecule of water in its shell, −1980 kJ/mol) and Co^{2+} (9.6 molecule of water in its shell, −1915 kJ/mol) which are also incompatible with the aragonite structure and which show lower Log $D^{2+}_{aragonite,\ eq}$ values than Zn^{2+} (i.e., −1.6) in the case of Ni^{2+} (i.e., −3.9) and higher in the case of Co^{2+} (i.e., −1.0). Nevertheless, the very high exchange rate of water molecules in the hydration shell of Zn ions (i.e., ~3×10^8 s^{-1}; Lincoln and Merbach, 1995) does not seem to correlate with the Log $D^{2+}_{aragonite,\ eq}$ found for Ni^{2+} and Co^{2+} which both show lower rate exchange of water molecule in the hydration shell (i.e., 3.15×10^4 and 3.18×10^6 s^{-1}, respectively).

Similar to the case of calcite, several studies attempted to model the Log $D^{2+}_{aragonite,\ eq}$ values following different approaches. Not surprisingly, the approach adopted by Böttcher and Dietzel, (2010) shows a value (−0.1) relatively far from that estimated in this work. Indeed, if this approach showed interesting estimations for the incorporation of elements compatible with the structure of the mineral, the absence of solid-solution formation between aragonite and smithsonite, which crystallizes in different systems (i.e., orthorhombic and trigonal, respectively), represents the main limitation in the use of this method. Interestingly, the approach of Wang and Xu (2001), proposing a value of Log $D^{2+}_{aragonite,\ eq} = 0.5$, also cannot explain the values estimated in this study. This difference between modelled and experimental values is not the first reported and has already been observed for Mg^{2+}, Ni^{2+} and Co^{2+} incorporation in aragonite or for Sr^{2+} incorporation in calcite (Rimstidt et al., 1998; Mavromatis et al., 2022; Brazier and Mavromatis, 2022). These results, as those for Zn^{2+} incorporation into calcite and aragonite, expose the difficulties of accurately modelling the elemental distribution coefficients in both calcite and aragonite and thus this study merge this gap of knowledge with experimental data.

4.3. Modelling the incorporation of Zn in calcite and aragonite

Several models explaining the elemental incorporation of foreign elements into calcite and aragonite have been proposed in the literature. In all cases, it appears that the rate of mineral growth is a parameter that is influencing the incorporation of ions either they are compatible or incompatible with the host mineral phase. For example, DePaolo (2011) proposed an approach based on the surface reaction kinetic model (SRKM) to describe the relationship between distribution coefficient of foreign ions into calcium carbonate minerals and mineral growth rate. In this model, which considers only the aqueous phase from which the mineral is precipitating, the distribution coefficients at thermodynamic equilibrium and as far as equilibrium as possible conditions are considered to describe mathematically the relationship between the distribution coefficient and the mineral growth rate as:

$$D_{Me} = \frac{D_f}{1 + \frac{R_b}{r_p + R_b} \times \left(\frac{D_f}{D_{eq}} - 1\right)} \quad (11)$$

where D_{Me} is the distribution coefficient of the foreign element between the considered mineral and the reactive fluid, D_{eq} the distribution coefficient of the considered element at thermodynamic equilibrium, D_f is the forward kinetic distribution coefficient, R_b the dissolution rate of the considered mineral (considered as constant when far from equilibrium), and r_p the growth rate of the considered mineral. Using this model DePaolo (2011) described, for example, the experimental trends of D_{Sr} or D_{Mn} as a function of growth rate during their incorporation into calcite (Lorens, 1981; Tesoriero and Pankow, 1996; Tang et al., 2008). These results demonstrate the ability of SRKM to quantitatively model the incorporation of elements that are compatible (in this case Mn^{2+}) and even incompatible (in this case Sr^{2+}) with the structure of the considered mineral. However, in a recent study Brazier and Mavromatis (2022) were unable to explain their experimental trends between D_{Ni} and D_{Co} and the mineral growth rate of aragonite without implying dissolution rate (R_b) values for aragonite far from the measured values found in literature.

Following this approach, the SRKM was fitted to the experimental data obtained for Zn when incorporated in calcite (compatible structure) and in aragonite (incompatible structure). The parameters used to fit the model to the data are presented in the Table 2, where both calcite and the Scenario 1 for aragonite use parameter values provided by literature data while a second scenario (Scenario 2) is proposed for aragonite because of the poor fit of the Scenario 1. In every case, it appears that the value of R_b is a critical parameter for the modelling. For calcite dissolution rate, Chou et al. (1989) proposed a value of $R_{b,calcite}$ of 10^{-6} mol/m^2/s at pH = 6.3 whereas in a more recent study Cubillas et al. (2005) proposed a value of $R_{b,calcite}$ of $10^{-6.5}$ for pH = 6.3. This difference likely arises from the estimation method of the specific surface area of the mineral between the two studies; Chou et al. (1989) used geometry and average grain size whereas Cubillas et al. (2005) used BET

Table 2
Values of R_b, D_{eq} and D_f chosen to fit our experimental D^{2+}_{Zn} between calcite and aragonite and the reactive fluid with the SRKM model.

Parameters	Zn in calcite	Zn in aragonite	
		Scenario 1	*Scenario 2*
R_b	$10^{-6.5}$*	$10^{-6.3}$*	10^{-9}
D_{eq}	$10^{1.9}$**	$10^{-1.6}$**	$10^{-1.6}$**
D_f	3.5	0.8	0.8

* From Cubillas et al., 2005.
** Calculated from Eqs. (7) and (10) using a $SI_{calcite}$ and $SI_{aragonite}$ = 0, respectively.

measurements. Furthermore, in their study Cubillas et al. (2005) compared their dissolution rates to the method used to estimate the specific surface area (BET vs. geometric estimation) and showed differences of almost 1 order of magnitude on the dissolution rates between the two methods, indicating that the geometric estimation of the specific surface area is a source of significant error on the dissolution rate estimation. In this work a $R_{b,calcite}$ value of $10^{-6.5}$ mol/m^2/s is used to model the incorporation of Zn into calcite. A value of $D_{eq} = 10^{1.9}$ was chosen reflecting $SI_{calcite} = 0$ according to Eq. (7). The value of D_f was chosen to fit the experimental data and was set to 3.5. The results (Fig. 6A) indicate that the SRKM fits very well the experimental D^{2+}_{Zncite} values, reflecting data that are in transition state between equilibrium and pure kinetic conditions.

Using the same approach for aragonite, the value of $R_{b,\ aragonite} = 10^{-6.3}$ proposed by Cubillas et al. (2005) for a pH = 6.3 was selected for the Scenario 1 (see Table 2). The D_{eq} was set at $10^{-1.6}$ and the D_f was set to 0.8. The results of Scenario 1 (Fig. 6B) show that the SRKM does not fit the data. Interestingly a suitable fit is obtained only when $R_{b,\ aragonite}$ is set to a value of 10^{-9} (see Scenario 2, Table 2 and Fig. 6C). This 2.7 orders of magnitude difference between the measured $R_{b,\ aragonite}$ value (Cubillas et al., 2005) and the one used in Scenario 2 to fit our experimental data (Table 2) is surprising. This discrepancy however comes in agreement with the observations by Brazier and Mavromatis (2022) who showed that R_b values significantly lower than $10^{-6.3}$ (Cubillas et al., 2005) are required to model D_{Ni} and D_{Co} in aragonite using the SRKM. In contrast to these two ions, Zn is known to have a significant inhibiting effect on aragonite dissolution (Gutjahr et al., 1996), but it seems unlikely that this process could explain the very low values needed for the SRKM to fit our data as a similar effect should be noticed for $R_{b,\ calcite}$.

It is likely that the inability of SRKM to fit the incorporation of Zn in aragonite is related to the absence of formation of a solid-solution system. Indeed, in the case of calcite although Zn is initially sorbed on this mineral surface as tetrahedral species (Elzinga and Reeder, 2002), it increases its coordination to 6 ideally substituting Ca and forming a diluted solid-solution (Reeder et al., 1999). Likely both the rate of dehydration of the 6-coordinated Zn^{2+}(aq) ion and the rate of coordination change from 4 in the adsorbed species to 6 in the incorporated ion are limiting factors of the incorporation of Zn in calcite which is reduced at higher mineral growth rates. In contrast, not much is known about the adsorption of Zn in aragonite but it is very likely that incorporation is favoured by the density of defect sites (e.g., vacancies, dislocations,

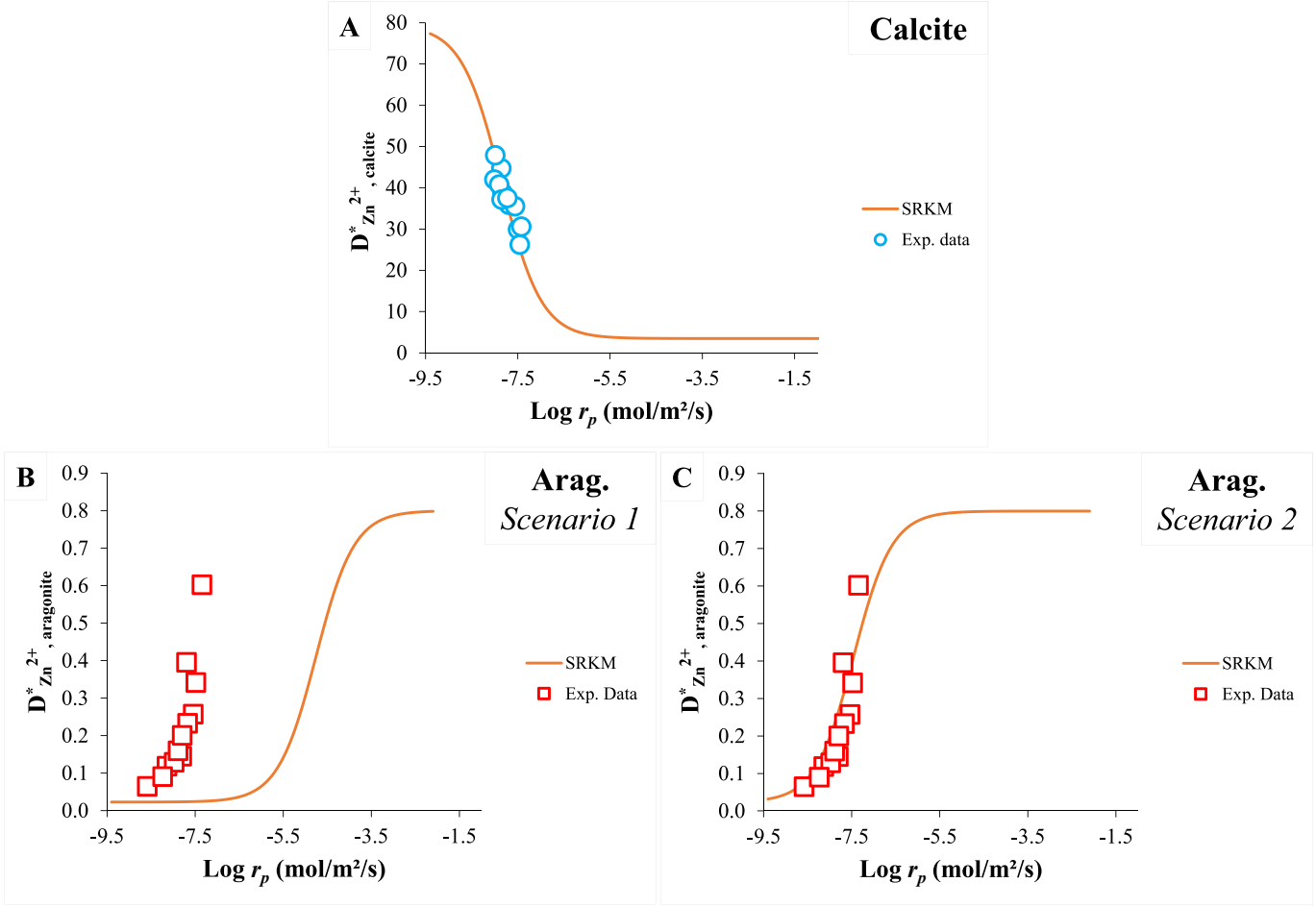

Fig. 6. Experimental distribution coefficients $D^{2+}_{Zncalcite}$ (blue circle) and $D^{2+}_{Znragonite}$ (red square) plotted against mineral growth rate (Log r_p) in comparison to the SRKM model predictions (orange curve). The parameters used for the SRKM models are given in Table 2. (For interpretation of the references to colour in this figure legend, the reader is referred to the web version of this article.)

stacking faults) on the mineral surface. Indeed, a similar behaviour has been shown for many elements that are incompatible with the structure of the minerals in which they have been experimentally incorporated (e.g., Li^{+}, Na^{+}, Mg^{2+}, Ni^{2+}, Co^{2+}) (Busenberg and Plummer, 1985; Füger et al., 2019; Brazier and Mavromatis, 2022; Mavromatis et al., 2022). It was for example shown that ion attachment, in the case of calcite, occurs mainly at defect sites generating spiral growths up to surface nucleation when the saturation index of the fluid with respect to the precipitating mineral increase (Teng et al., 2000). Consequently, it is suggested that the concentration of defect sites on the mineral surface and therefore the amount of moles of incompatible elements with the mineral structure adsorbed and incorporated are also driven by the saturation state of the reactive fluid. Nevertheless, the form under which Zn is incorporated into aragonite remains questionable.

4.4. Implications for natural environments

The results of this study show that the incorporation of Zn in both calcite and aragonite is strongly dependent on the mineral growth rate and also on the saturation state of the reactive fluid with respect to the mineral forming. Interestingly, this effect seems to be more pronounced for aragonite than for calcite as highlighted by the larger slopes in Eqs. (6) and (10) compared to Eqs. (5) and (7). These trends suggest that the Zn/Ca ratio of carbonate minerals may be a proxy for the mineral growth rate and the saturation index of the reactive fluid with respect to calcite or aragonite. It should be noted, however, that the application of our results to natural environments, in particular oceanic waters, remains challenging as (i) the saturation state with respect to calcite and aragonite of the reactive fluid explored in this study are lower than the one of natural seawater, (ii) major ions such as SO_4^{2-} and Mg^{2+} (for the calcite experiments) that are known to affect the elemental incorporation into carbonates are not present in the experiments, (iii) the experiments in this study were performed in nitrate background electrolyte and at pH ~6.3, which is highly different than the seawater conditions (i.e., pH ~8–8.3 and high chloride content) and have thus an important impact on the Zn speciation, and (iv) in the case of biomineralization, the presence of organic compounds can highly affect the incorporation (e.g., Mucci and Morse, 1983; Busenberg and Plummer, 1985; Cohen and McConnaughey, 2003; Feely et al., 2009; Goetschl et al., 2019). Nevertheless, previous studies already highlighted a correlation between the Zn/Ca ratio of the carbonate minerals and the physico-chemical parameters of the reactive fluids from which they precipitate. For example, Marchitto Jr et al. (2000), Marchitto et al. (2005) showed a positive correlation between the D_{Zn} in benthic foraminifera (*Cibicidoides wuellerstorfi*) and the degree of saturation of the seawater from which they precipitated. Interestingly, these results exhibit an opposite trend to that of the present study. This unusual behaviour was explained by an incorporation of trace metals during calcification through a Rayleigh distillation from an internal biomineralization reservoir of the foraminifer. When the saturation state of the water decreases, the foraminifer tends to use more this reservoir. It seems therefore that biological effects, and potentially complexation of Zn with organic compounds, are the cause of the differences between inorganic experiments and biomineralization processes. In a more recent study, van Dijk et al. (2017) cultured Ammonia *tepida* foraminifera in a medium highly supersaturated with respect to calcite (up to $SI_{calcite} = 1.41$) and showed similar trends to the present study with D_{Zn} values decreasing with increasing saturation of the fluid with respect to calcite. Nevertheless, it has to be noted that at such high $SI_{calcite}$, nucleation effects cannot be entirely excluded. Interestingly, they also show that the measured D_{Zn} values in the literature for different foraminiferal species (i.e. *Cibicidoides wuellerstorfi*, Cibicidoides *pachyderma*, Pseudotriloculina *rotunda*, Ammonia *tepida*) are in the range of 0.2–22, which is lower than the value measured in this work, and are even problematic for D_{Zn} values lower than 1 which go against the limitation dictated by thermodynamic considerations for elements compatible with the structure of the mineral in which they are incorporated (Marchitto Jr et al., 2000; Bryan and Marchitto, 2010; Nardelli et al., 2016). The differences to this study likely arise from two sources: (1) biological effects that will have a strong effect on Zn speciation and its incorporation into bio-controlled or bio-induced carbonates, and/or (2) mineral growth rates that are much higher for biological calcite than those investigated in this work and will therefore generate much lower D_{Zn}. In all cases, it appears that the D_{Zn}, even in a natural environment, is controlled at least partially by the supersaturation of the fluid with respect to the considered carbonate mineral and thus by the mineral growth rate. These results seem promising for the establishment of a proxy based on the Zn/Ca ratio in carbonate minerals but require further investigation in order to provide robust calibrations for its use.

On the continental domain, trace element incorporation into speleothem have shown great potential as tracer of local (paleo)environmental conditions (e.g., Wassenburg et al., 2020; Baldini et al., 2015; Oster et al., 2017, 2020; Giesche et al., 2023; Griffiths et al., 2010). In contrast to environments where the fluid represents an almost infinite component (e.g., the ocean), the precipitation of calcite/aragonite speleothem (calcite being the dominant phase because of its thermodynamic stability) is highly dependent on the drip water availability, evolution and composition. The drip water availability and evolution are mostly related to the seasonality (i.e., alternation between dry and wet seasons) and the local conditions of rainfall origin and (ground) water-rock interaction. Thus, the element concentrations in speleothem respond to a succession of individual and coupled parameters that affect the composition of the drip water from which the speleothem is precipitating, including for example the host rock composition, the incongruent dissolution of calcite (i.e., ICD), the temperature, the potential prior calcite or aragonite precipitation (i.e., PCP or PAP, respectively), the water residence time in the aquifer, the CO_2 content in the covering soil horizons and in the cave, the affinity of ions to be adsorbed onto solid surfaces, and the presence of aqueous organic ligands (e.g., Fairchild et al., 2000; Wassenburg et al., 2013, 2016, 2020; Griffiths et al., 2010; Sinclair, 2011; Sherwin and Baldini, 2011; Fairchild and Treble, 2009). Zinc ions are often considered as soil-derived because of their strong affinity to adsorption on negatively charged soil components. Accordingly, Zn concentration in ground and drip water is controlled by the flushing of soils and transport of either aqueous species or organics colloids/particulate on which the Zn^{2+} is adsorbed (e.g., Borsato et al., 2007). The variable composition of naturally occurring drip water makes it difficult to be directly compared to the results of this study performed under inorganic conditions, with a constant pH and a higher ionic strength compared to common drip water, and with a constant supply of Zn ions. Nevertheless, Wassenburg et al. (2016) reported for example a decrease of D_{Sr} for aragonitic speleothem with increasing extension rate that is in adequation with results published during abiotic aragonite growth experiments (e.g., Dietzel et al., 2004; Brazier et al., 2023). If a similar relationship is assumed for D_{Zn} and growth rate, it therefore appears that following the Eqs. (5 and 6), the D_{Zn} could be used as a proxy of aragonite (or calcite) growth rate. Such an application assumes to have a reasonable knowledge of the composition of the drip water, and at least short-time scale homogeneity of the drip water composition and a non-significant effect of organics on the calcite/aragonite formation under the defined natural conditions. Indeed, it must be noted that the composition and physico-chemical parameters of the drip water are usually responding to rapid environmental changes, it is therefore difficult to suggest that the growth rate is the only or the main driver of incorporation of Zn ions into speleothems over a long period of time.

As a potential perspective, calculating a ΔD_{Zn}^{2+} ($\Delta D_{Zn}^{2+} = D_{Zn_{calcite}}^{2+} - D_{Zn_{aragonite}}^{2+}$) on natural samples that are composed of an assemblage of calcite and aragonite (for which the proportion are known or reasonably assumed) could provide a rough estimation of the growth rate (close or far from equilibrium). In fact, the more the solids will grow far from equilibrium the more the ΔD_{Zn}^{2+} will be small and close to zero. This ΔD_{Zn}^{2+}

could then represent an indicator of growth rate independent of the solution chemistry if a similar growth rate for calcite and aragonite can be assumed.

5. Conclusion

The results of this study show Zn ions to be incorporated into calcite and aragonite at a high and low amount, respectively. The compatibility of Zn for calcite structure indicates an incorporation of Zn^{2+} by ion-by-ion substitution with the Ca^{2+} with formation of a diluted solid-solution between the endmember minerals calcite and smithsonite. In contrast, the incompatibility of Zn for aragonite indicates a lack of substitution of Zn^{2+} with Ca^{2+}. It appears that other physico-chemical properties of Zn ions, such as hydration energy, the number of water molecules in the first hydration shell and/or the exchange rate of water molecules in the hydration sphere, may play a decisive role in the incorporation behaviour of Zn in aragonite and, in particular, in its dependence on the growth rate. Interestingly, important correlations between the D^{2+}_{Zn} and the saturation indices of the reactive fluid with respect to calcite and aragonite were also recognized in this work. These dependencies allowed to define two linear mathematical relations between D^{2+}_{Zn} and saturation indices with respect to calcite and aragonite and thus to estimate D^{2+}_{Zn} by considering SI = 0 ($D^{2+}_{Zn\,calcite,\ eq} = 10^{1.9}$ and $D^{2+}_{Zn\,aragonite,\ eq} = 10^{-1.6}$). This values for calcite is relatively close to those calculated using an approach correlating the $D^{2+}_{Zn\,calcite,\ eq}$ to the K_{Sp} of the end-members (i.e., calcite and smithsonite) but is much higher than those calculated by considering the ionic radii, the Gibbs free energy of formation and the standard non-solvation energy. In the case of aragonite, our estimated value of $D^{2+}_{Zn\,aragonite,\ eq}$ is much lower than those previously proposed in the literature, raising thus the problems related to the estimation of $D_{Me,\ eq}$ for ions incompatible with the structure of the host mineral. For both calcite and aragonite, the dependencies between D^{2+}_{Zn} and growth rate and D^{2+}_{Zn} and SI of the reactive fluid with respect to the considered mineral suggests the interest of D^{2+}_{Zn} as a proxy for these two metrics.

It appears that our experimental data can be explained very well by the Surface Reaction Kinetic Model (SRKM) concerning the evolution of $D^{2+}_{Zn\,\mathrm{calcite}}$ with the growth rate using parameters commonly accepted in the literature. Nevertheless, the SRKM is unable to explain our experimental data for aragonite without invoking much lower dissolution rate values than the one experimentally determined by previous studies. These results highlight our difficulty to model the incorporation of Zn^{2+} in aragonite, which is probably dependent on the density of defect sites on the mineral surface, itself closely related to the saturation index of the reactive fluid with respect to aragonite. The form in which Zn is incorporated into aragonite remains still enigmatic and requires ongoing research.

Declaration of Competing Interest

The authors declare the following financial interests/personal relationships which may be considered as potential competing interests:

Jean-Michel Brazier reports financial support was provided by Austrian Science Fund. Jean-Michel Brazier reports a relationship with Austrian Science Fund that includes: funding grants.

Data availability

Data will be made available on request.

Acknowledgments

We thank Bettina Purgstaller for her technical support. For their assistance with BET and SEM analyses, we are thankful to Anna Harrison and to Gerald Auer. This study was funded by the Austrian Science Fund (FWF) through the project P31832-N29.

Appendix A. Supplementary data

Supplementary data to this article can be found online at https://doi.org/10.1016/j.chemgeo.2023.121821.

References

Alvarez, C.C., Quitté, G., Schott, J., Oelkers, E.H., 2021. Nickel isotope fractionation as a function of carbonate growth rate during Ni coprecipitation with calcite. Geochim. Cosmochim. Acta 299, 184–198.
Baldini, L.M., McDermott, F., Baldini, J.U., Arias, P., Cueto, M., Fairchild, I.J., Hoffmann, D.L., Mattey, D.P., Müller, W., Nita, D.C., Ontañón, R., Garciá-Moncó, C., Richards, D.A., 2015. Regional temperature, atmospheric circulation, and sea-ice variability within the Younger Dryas Event constrained using a speleothem from northern Iberia. Earth Planet. Sci. Lett. 419, 101–110.
Bénézeth, P., Saldi, G.D., Dandurand, J.L., Schott, J., 2011. Experimental determination of the solubility product of magnesite at 50 to 200 C. Chem. Geol. 286 (1–2), 21–31.
Berner, R.A., 1975. The role of magnesium in the crystal growth of calcite and aragonite from sea water. Geochim. Cosmochim. Acta 39 (4), 489–504.
Bischoff, J.L., 1968. Kinetics of calcite nucleation: magnesium ion inhibition and ionic strength catalysis. J. Geophys. Res. 73 (10), 3315–3322.
Bong, C.W., Malfatti, F., Azam, F., Obayashi, Y., Suzuki, S., 2010. The effect of zinc exposure on the bacteria abundance and proteolytic activity in seawater. In: Interdisciplinary Studies on Environmental Chemistry—Biological Responses to Contaminants. Terrapub, Tokyo, pp. 57–63.
Borsato, A., Frisia, S., Fairchild, I.J., Somogyi, A., Susini, J., 2007. Trace element distribution in annual stalagmite laminae mapped by micrometer-resolution X-ray fluorescence: implications for incorporation of environmentally significant species. Geochim. Cosmochim. Acta 71 (6), 1494–1512.
Böttcher, M.E., Dietzel, M., 2010. Metal-ion partitioning during low-temperature precipitation and dissolution of anhydrous carbonates and sulphates. Eur. Mineral. Union Notes Mineral. 10 (1), 139–187.
Brazier, J.M., Mavromatis, V., 2022. Effect of growth rate on nickel and cobalt incorporation in aragonite. Chem. Geol. 600, 120863.
Brazier, J.M., Blanchard, M., Méheut, M., Schmitt, A.D., Schott, J., Mavromatis, V., 2023. Experimental and theoretical investigations of stable Sr isotope fractionation during its incorporation in aragonite. Geochim. Cosmochim. Acta 358, 134–147.
Bruland, K.W., Lohan, M.C., 2006. Controls of trace metals in seawater. Oceans Marine Geochem. 6, 23–47.
Brunauer, S., Emmett, P.H., Teller, E., 1938. Adsorption of gases in multimolecular layers. J. Am. Chem. Soc. 60 (2), 309–319.
Bryan, S.P., Marchitto, T.M., 2010. Testing the utility of paleonutrient proxies Cd/ca and Zn/ca in benthic foraminifera from thermocline waters. Geochem. Geophys. Geosyst. 11 (1).
Burgess, J., Prince, R.H., 2006. Zinc: Inorganic & Coordination Chemistry. Encyclopedia of Inorganic Chemistry.
Burton, W.K., Cabrera, N., Frank, F.C., 1951. The growth of crystals and the equilibrium structure of their surfaces. Philos. Trans. Royal Soc. London. Series A, Math. Phys. Sci. 243 (866), 299–358.
Busenberg, E., Plummer, L.N., 1985. Kinetic and thermodynamic factors controlling the distribution of SO_3^{2-} and Na^+ in calcites and selected aragonites. Geochim. Cosmochim. Acta 49 (3), 713–725.
Cheng, L., Sturchio, N.C., Woicik, J.C., Kemner, K.M., Lyman, P.F., Bedzyk, M.J., 1998. High-resolution structural study of zinc ion incorporation at the calcite cleavage surface. Surf. Sci. 415 (1–2), L976–L982.
Chou, L.E.I., Garrels, R.M., Wollast, R., 1989. Comparative study of the kinetics and mechanisms of dissolution of carbonate minerals. Chem. Geol. 78 (3–4), 269–282.
Cohen, A.L., McConnaughey, T.A., 2003. Geochemical perspectives on coral mineralization. Rev. Mineral. Geochem. 54 (1), 151–187.
Conway, T.M., John, S.G., 2014. The biogeochemical cycling of zinc and zinc isotopes in the North Atlantic Ocean. Glob. Biogeochem. Cycles 28 (10), 1111–1128.
Crocket, J.H., Winchester, J.W., 1966. Coprecipitation of zinc with calcium carbonate. Geochim. Cosmochim. Acta 30 (10), 1093–1109.
Cubillas, P., Köhler, S., Prieto, M., Chaïrat, C., Oelkers, E.H., 2005. Experimental determination of the dissolution rates of calcite, aragonite, and bivalves. Chem. Geol. 216 (1–2), 59–77.
DePaolo, D.J., 2011. Surface kinetic model for isotopic and trace element fractionation during precipitation of calcite from aqueous solutions. Geochim. Cosmochim. Acta 75 (4), 1039–1056.
Dietzel, M., Gussone, N., Eisenhauer, A., 2004. Co-precipitation of Sr^{2+} and Ba^{2+} with aragonite by membrane diffusion of CO_2 between 10 and 50°C. Chem. Geol. 203 (1–2), 139–151.
Dong, S., Wasylenki, L.E., 2016. Zinc isotope fractionation during adsorption to calcite at high and low ionic strength. Chem. Geol. 447, 70–78.
Dromgoole, E.L., Walter, L.M., 1990. Iron and manganese incorporation into calcite: Effects of growth kinetics, temperature and solution chemistry. Chem. Geol. 81 (4), 311–336.
Elzinga, E.J., Reeder, R.J., 2002. X-ray absorption spectroscopy study of Cu^{2+} and Zn^{2+} adsorption complexes at the calcite surface: implications for site-specific metal incorporation preferences during calcite crystal growth. Geochim. Cosmochim. Acta 66 (22), 3943–3954.
Elzinga, E.J., Rouff, A.A., Reeder, R.J., 2006. The long-term fate of Cu^{2+}, Zn^{2+}, and Pb^{2+} adsorption complexes at the calcite surface: an X-ray absorption spectroscopy study. Geochim. Cosmochim. Acta 70 (11), 2715–2725.

Fairchild, I.J., Treble, P.C., 2009. Trace elements in speleothems as recorders of environmental change. Quat. Sci. Rev. 28 (5–6), 449–468.
Fairchild, I.J., Borsato, A., Tooth, A.F., Frisia, S., Hawkesworth, C.J., Huang, Y., McDermott, F., Spiro, B., 2000. Controls on trace element (Sr–Mg) compositions of carbonate cave waters: implications for speleothem climatic records. Chem. Geol. 166 (3–4), 255–269.
Feely, R.A., Doney, S.C., Cooley, S.R., 2009. Ocean acidification: present conditions and future changes in a high-CO_2 world. Oceanography 22 (4), 36–47.
Fisher, N.S., Jones, G.J., Nelson, D.M., 1981. Effects of copper and zinc on growth, morphology, and metabolism of Asterionella japonica (Cleve) 1. J. Exp. Mar. Biol. Ecol. 51 (1), 37–56.
Frost, R.L., Martens, W.N., Wain, D.L., Hales, M.C., 2008. Infrared and infrared emission spectroscopy of the zinc carbonate mineral smithsonite. Spectrochim. Acta A Mol. Biomol. Spectrosc. 70 (5), 1120–1126.
Füger, A., Konrad, F., Leis, A., Dietzel, M., Mavromatis, V., 2019. Effect of growth rate and pH on lithium incorporation in calcite. Geochim. Cosmochim. Acta 248, 14–24.
Fujii, T., Moynier, F., Blichert-Toft, J., Albarède, F., 2014. Density functional theory estimation of isotope fractionation of Fe, Ni, Cu, and Zn among species relevant to geochemical and biological environments. Geochim. Cosmochim. Acta 140, 553–576.
Gabitov, R.I., Gaetani, G.A., Watson, E.B., Cohen, A.L., Ehrlich, H.L., 2008. Experimental determination of growth rate effect on U^{6+} and Mg^{2+} partitioning between aragonite and fluid at elevated U^{6+} concentration. Geochim. Cosmochim. Acta 72 (16), 4058–4068.
Gabitov, R.I., Schmitt, A.K., Rosner, M., McKeegan, K.D., Gaetani, G.A., Cohen, A.L., Watson, E.B., Harrison, T.M., 2011. In situ δ^7Li, Li/Ca, and Mg/Ca analyses of synthetic aragonites. Geochem. Geophys. Geosyst. 12 (3).
Gabitov, R.I., Sadekov, A., Dyer, J., Perez-Huerta, A., Xu, H., Migdisov, A., 2021. Sectoral and growth rate control on elemental uptake by individual calcite crystals. Chem. Geol. 585, 120589.
Gaetani, G.A., Cohen, A.L., 2006. Element partitioning during precipitation of aragonite from seawater: a framework for understanding paleoproxies. Geochim. Cosmochim. Acta 70 (18), 4617–4634.
Gautier, Q., Bénézeth, P., Mavromatis, V., Schott, J., 2014. Hydromagnesite solubility product and growth kinetics in aqueous solution from 25 to 75°C. Geochim. Cosmochim. Acta 138, 1–20.
Giesche, A., Hodell, D.A., Petrie, C.A., Haug, G.H., Adkins, J.F., Plessen, B., Marwan, N., Bradbury, H.J., Hartland, A., French, A.D., Breitenbach, S.F., 2023. Recurring summer and winter droughts from 4.2-3.97 thousand years ago in North India. Commun. Earth Environ. 4 (1), 103.
Goetschl, K.E., Purgstaller, B., Dietzel, M., Mavromatis, V., 2019. Effect of sulfate on magnesium incorporation in low-magnesium calcite. Geochim. Cosmochim. Acta 265, 505–519.
Griffiths, M.L., Drysdale, R.N., Gagan, M.K., Frisia, S., Zhao, J.X., Ayliffe, L.K., Hantoro, W.S., Hellstrom, J.C., Fischer, M.J., Feng, Y.-X., Suwargadi, B.W., 2010. Evidence for Holocene changes in Australian–Indonesian monsoon rainfall from stalagmite trace element and stable isotope ratios. Earth Planet. Sci. Lett. 292 (1–2), 27–38.
Gutjahr, A., Dabringhaus, H., Lacmann, R., 1996. Studies of the growth and dissolution kinetics of the $CaCO_3$ polymorphs calcite and aragonite II. The influence of divalent cation additives on the growth and dissolution rates. J. Cryst. Growth 158 (3), 310–315.
Harrison, A.L., Mavromatis, V., Oelkers, E.H., Bénézeth, P., 2019. Solubility of the hydrated Mg-carbonates nesquehonite and dypingite from 5 to 35°C: Implications for CO_2 storage and the relative stability of Mg-carbonates. Chem. Geol. 504, 123–135.
Kaur, H., Garg, N., 2021. Zinc toxicity in plants: a review. Planta 253 (6), 1–28.
Kitano, Y., Kanamori, N., Tokuyama, A., Comori, T., 1973. Factors controlling the trace-element contents of marine carbonate skeletons. In: Proceeding of Symposium on Hydrogeochemistry and Biogeochemistry, The Clarke Co, Washington, DC, pp. 484–499.
Kitano, Y., Okumura, M., Idogaki, M., 1975. Incorporation of sodium, chloride and sulfate with calcium carbonate. Geochem. J. 9 (2), 75–84.
Kitano, Y., Kanamori, N., Yoshioka, S., 1976. Adsorption of zinc and copper ions on calcite and aragonite and its influence on the transformation of aragonite to calcite. Geochem. J. 10 (4), 175–179.
Kitano, Y., Sakata, M., Matsumoto, E., 1980. Partitioning of heavy metals into mineral and organic fractions in a sediment core from Tokyo Bay. Geochim. Cosmochim. Acta 44 (9), 1279–1285.
Lakshtanov, L.Z., Stipp, S.L.S., 2007. Experimental study of nickel (II) interaction with calcite: Adsorption and coprecipitation. Geochim. Cosmochim. Acta 71 (15), 3686–3697.
Lee, Y.J., Reeder, R.J., 2006. The role of citrate and phthalate during Co (II) coprecipitation with calcite. Geochim. Cosmochim. Acta 70 (9), 2253–2263.
Lincoln, S.F., Merbach, A.E., 1995. Substitution reactions of solvated metal ions. Adv. Inorg. Chem. 42, 1–88.
Lorens, R.B., 1981. Sr, Cd, Mn and Co distribution coefficients in calcite as a function of calcite precipitation rate. Geochim. Cosmochim. Acta 45 (4), 553–561.
Marchitto Jr., T.M., Curry, W.B., Oppo, D.W., 2000. Zinc concentrations in benthic foraminifera reflect seawater chemistry. Paleoceanography 15 (3), 299–306.
Marchitto, T.M., Lynch-Stieglitz, J., Hemming, S.R., 2005. Deep Pacific $CaCO_3$ compensation and glacial–interglacial atmospheric CO_2. Earth Planet. Sci. Lett. 231 (3–4), 317–336.
Marcus, Y., 1991. Thermodynamics of solvation of ions. Part 5.—Gibbs free energy of hydration at 298.15 K. J. Chem. Soc. Faraday Trans. 87 (18), 2995–2999.
Mavromatis, V., Gautier, Q., Bosc, O., Schott, J., 2013. Kinetics of Mg partition and Mg stable isotope fractionation during its incorporation in calcite. Geochim. Cosmochim. Acta 114, 188–203.
Mavromatis, V., Montouillout, V., Noireaux, J., Gaillardet, J., Schott, J., 2015. Characterization of boron incorporation and speciation in calcite and aragonite from co-precipitation experiments under controlled pH, temperature and precipitation rate. Geochim. Cosmochim. Acta 150, 299–313.
Mavromatis, V., Goetschl, K.E., Grengg, C., Konrad, F., Purgstaller, B., Dietzel, M., 2018. Barium partitioning in calcite and aragonite as a function of growth rate. Geochim. Cosmochim. Acta 237, 65–78.
Mavromatis, V., González, A.G., Dietzel, M., Schott, J., 2019. Zinc isotope fractionation during the inorganic precipitation of calcite–Towards a new pH proxy. Geochim. Cosmochim. Acta 244, 99–112.
Mavromatis, V., Brazier, J.M., Goetschl, K.E., 2022. Controls of temperature and mineral growth rate on Mg incorporation in aragonite. Geochim. Cosmochim. Acta 317, 53–64.
McIntire, W.L., 1963. Trace element partition coefficients—a review of theory and applications to geology. Geochim. Cosmochim. Acta 27 (12), 1209–1264.
Morel, F.M., Price, N.M., 2003. The biogeochemical cycles of trace metals in the oceans. Science 300 (5621), 944–947.
Morse, J.W., Bender, M.L., 1990. Partition coefficients in calcite: Examination of factors influencing the validity of experimental results and their application to natural systems. Chem. Geol. 82, 265–277.
Mucci, A., Morse, J.W., 1983. The incorporation of Mg^{2+} and Sr^{2+} into calcite overgrowths: influences of growth rate and solution composition. Geochim. Cosmochim. Acta 47 (2), 217–233.
Nardelli, M.P., Malferrari, D., Ferretti, A., Bartolini, A., Sabbatini, A., Negri, A., 2016. Zinc incorporation in the miliolid foraminifer *Pseudotriloculina rotunda* under laboratory conditions. Mar. Micropaleontol. 126, 42–49.
Okumura, M., Kitano, Y., 1986. Coprecipitation of alkali metal ions with calcium carbonate. Geochim. Cosmochim. Acta 50 (1), 49–58.
Oster, J.L., Sharp, W.D., Covey, A.K., Gibson, J., Rogers, B., Mix, H., 2017. Climate response to the 8.2 ka event in coastal California. Sci. Rep. 7 (1), 3886.
Oster, J.L., Weisman, I.E., Sharp, W.D., 2020. Multi-proxy stalagmite records from northern California reveal dynamic patterns of regional hydroclimate over the last glacial cycle. Quat. Sci. Rev. 241, 106411.
Paquette, J., Reeder, R.J., 1995. Relationship between surface structure, growth mechanism, and trace element incorporation in calcite. Geochim. Cosmochim. Acta 59 (4), 735–749.
Parkhurst, D.L., Appelo, C.A.J., 2013. Description of Input and Examples for PHREEQC Version 3: A Computer Program for Speciation, Batch-Reaction, One-Dimensional Transport, and Inverse Geochemical Calculations (No. 6-A43). US Geological Survey.
Raiswell, R., Brimblecombe, P., 1977. The partition of manganese into aragonite between 30 and 60°C. Chem. Geol. 19 (1–4), 145–151.
Reeder, R.J., 1996. Interaction of divalent cobalt, zinc, cadmium, and barium with the calcite surface during layer growth. Geochim. Cosmochim. Acta 60 (9), 1543–1552.
Reeder, R.J., Lamble, G.M., Northrup, P.A., 1999. XAFS study of the coordination and local relaxation around Co^{2+}, Zn^{2+}, Pb^{2+}, and Ba^{2+} trace elements in calcite. Am. Mineral. 84 (7–8), 1049–1060.
Rimstidt, J.D., Balog, A., Webb, J., 1998. Distribution of trace elements between carbonate minerals and aqueous solutions. Geochim. Cosmochim. Acta 62 (11), 1851–1863.
Rout, G.R., Das, P., 2009. Effect of metal toxicity on plant growth and metabolism: I. Zinc. In: In Sustainable Agriculture. Springer, Dordrecht, pp. 873–884.
Shannon, R.D., 1976. Revised effective ionic radii and systematic studies of interatomic distances in halides and chalcogenides. Acta Crystallogr. Sect. A: Cryst. Phys., Diffr., Theor. Gen. Crystallogr. 32 (5), 751–767.
Sherwin, C.M., Baldini, J.U., 2011. Cave air and hydrological controls on prior calcite precipitation and stalagmite growth rates: Implications for palaeoclimate reconstructions using speleothems. Geochim. Cosmochim. Acta 75 (14), 3915–3929.
Sinclair, D.J., 2011. Two mathematical models of Mg and Sr partitioning into solution during incongruent calcite dissolution: implications for dripwater and speleothem studies. Chem. Geol. 283 (3–4), 119–133.
Tang, J., Köhler, S.J., Dietzel, M., 2008. Sr^{2+}/Ca^{2+} and $^{44}Ca/^{40}Ca$ fractionation during inorganic calcite formation: I. Sr incorporation. Geochim. Cosmochim. Acta 72 (15), 3718–3732.
Temmam, M., Paquette, J., Vali, H., 2000. Mn and Zn incorporation into calcite as a function of chloride aqueous concentration. Geochim. Cosmochim. Acta 64 (14), 2417–2430.
Teng, H.H., Dove, P.M., De Yoreo, J.J., 2000. Kinetics of calcite growth: surface processes and relationships to macroscopic rate laws. Geochim. Cosmochim. Acta 64 (13), 2255–2266.
Terakado, Y., Masuda, A., 1988. The coprecipitation of rare-earth elements with calcite and aragonite. Chem. Geol. 69 (1–2), 103–110.
Tesoriero, A.J., Pankow, J.F., 1996. Solid solution partitioning of Sr^{2+}, Ba^{2+}, and Cd^{2+} to calcite. Geochim. Cosmochim. Acta 60 (6), 1053–1063.
van Dijk, I., de Nooijer, L.J., Wolthers, M., Reichart, G.J., 2017. Impacts of pH and $[CO_3^{2-}]$ on the incorporation of Zn in foraminiferal calcite. Geochim. Cosmochim. Acta 197, 263–277.
Voigt, M., Mavromatis, V., Oelkers, E.H., 2017. The experimental determination of REE partition coefficients in the water-calcite system. Chem. Geol. 462, 30–43.
Wang, Y., Xu, H., 2001. Prediction of trace metal partitioning between minerals and aqueous solutions: a linear free energy correlation approach. Geochim. Cosmochim. Acta 65 (10), 1529–1543.
Wassenburg, J.A., Immenhauser, A., Richter, D.K., Niedermayr, A., Riechelmann, S., Fietzke, J., Scholz, D., Jochum, K.P., Fohlmeister, J., Schröder-Ritzrau, A.,

Sabaoui, A., Riechelmann, D.F.C., Esper, J., 2013. Moroccan speleothem and tree ring records suggest a variable positive state of the North Atlantic Oscillation during the Medieval Warm Period. Earth Planet. Sci. Lett. 375, 291–302.
Wassenburg, J.A., Scholz, D., Jochum, K.P., Cheng, H., Oster, J., Immenhauser, A., Richter, D.K., Häger, T., Jamieson, R.A., Baldini, J.U.L., Hoffmann, D., Breitenbach, S.F.M., 2016. Determination of aragonite trace element distribution coefficients from speleothem calcite–aragonite transitions. Geochim. Cosmochim. Acta 190, 347–367.
Wassenburg, J.A., Riechelmann, S., Schröder-Ritzrau, A., Riechelmann, D.F., Richter, D. K., Immenhauser, A., Terente, M., Constantin, S., Hachenberg, A., Hansen, M., Scholz, D., 2020. Calcite Mg and Sr partition coefficients in cave environments: Implications for interpreting prior calcite precipitation in speleothems. Geochim. Cosmochim. Acta 269, 581–596.
Weber, T., John, S., Tagliabue, A., DeVries, T., 2018. Biological uptake and reversible scavenging of zinc in the global ocean. Science 361 (6397), 72–76.
White, A.F., 1977. Sodium and potassium coprecipitation in aragonite. Geochim. Cosmochim. Acta 41 (5), 613–625.
Zachara, J.M., Kittrick, J.A., Dake, L.S., Harsh, J.B., 1989. Solubility and surface spectroscopy of zinc precipitates on calcite. Geochim. Cosmochim. Acta 53 (1), 9–19.